Int. J. Electrochem. Sci., 17 **(2022)** Article Number: 2212109, doi: 10.20964/2022.12.111

International Journal of
ELECTROCHEMICAL
SCIENCE
www.electrochemsci.org

A Novel ADEKF Method for State-of-Charge Estimation of Li-ion Batteries

Shanshan Chang, Ling Mao[*]*, Jinbin Zhao, Keqing Qu, Fen Li*

College of Electrical Engineering, Shanghai University of Electric Power, Shanghai 200090, China
[*]E-mail: maoling2290@shiep.edu.cn

Received: 7 November 2022/ *Accepted:* 15 December 2022/ *Published:* 27 December 2022

The capacity and state of charge (SOC) of a battery are essential for the battery management system (BMS). To perform high-accuracy online estimation of a battery throughout its life cycle, a joint estimator of SOC and capacity with low computational complexity based on an adaptive extended Kalman filter with a subregional decay element (ADEKF) is proposed in this paper. First, the parameters of the first-order circuit model are identified using the varied forgetting factor with recursive least squares (VFFRLS), and the simplified reduced-order equation of state for the battery is derived. Subsequently, the innovative ADEKF algorithm is proposed to adapt the simplified reduced-order state equation to achieve stable convergence of the SOC and capacity. Finally, the accuracy and adaptability of joint estimation with different initial states are verified using federal city driving program tests at 0 °C, 25 °C, and 45 °C for the optimal battery operating charge interval. In addition, compared with the other joint estimation methods, the results show that the proposed algorithm has much better performance in terms of joint estimation accuracy and convergence speed.

Keywords: Li-ion batteries; State-of-charge; Temperature; Kalman filter; Robustness analysis

1. INTRODUCTION

Lithium batteries are widely used in electric vehicles, grid energy storage systems, or other portable electronic devices for their superior performance, discharge stability, high energy density, and low cost [1]. Electrical vehicles are developing rapidly as part of countries' responses to ecological environment and energy security issues. An efficient and robust BMS is essential to ensure safe battery operation, long battery life, and economy. Currently, the two main tasks of the BMS are to accurately estimate the capacity and state of charge of lithium-ion batteries [2]. The first predicts the remaining battery life and power to avoid overcharging. The second characterizes the aging state of the battery, which gradually decreases to 80% of the rated capacity with prolonged use. However, not only can these

rarely be determined from battery measurements, but they are also affected by ambient temperature and aging, which makes the estimation of SOC and capacity a challenge in practical applications [3].

The SOC is an operational indicator for an electric vehicle. Accurate estimation of the SOC helps to determine the stable operating conditions of the battery and to inform the battery charging strategy. The main existing SOC estimation methods are divided into non-model-based and model-based methods. Among them, the non-model-based methods include the amperage-time integration method, the open circuit voltage (OCV) method, and the data-based method. The accuracy of the amperage-time integration method is largely dependent on the exact initial value of the battery and the ambient noise [4]. The open-circuit voltage method derives the SOC from the experimentally measured relationship between the SOC and OCV. The accuracy of the estimate is determined by the accuracy of the experiment. However, the experiments for acquiring OCV are time-consuming and have limited depolarization capability, so the method is not suitable for online SOC estimation [5]. The data-driven approach does not require modeling but establishes and trains from data such as voltage and temperature to form a matching relationship with the battery SOC to produce the estimate. However, it has a high computational cost and is unsuitable for real-world electric vehicle driving [6]. Therefore, the equivalent circuit model (ECM) of the battery model-based methods has been widely used, as it balances computation requirements and performance. Essentially, the ECM-based approach uses state estimation algorithms to achieve an optimal fusion of the ampere-time integration method and the open circuit voltage method [7]. This has driven the search for higher accuracy and a lower computational burden and led to an expansion of the available filters and observers, including the Kalman filter [8], sliding mode observer and moving time domain estimation. It should be noted that the Kalman filter algorithm is the most popular method for model-based estimation for SOC. For this algorithm, both measurement and process noise covariance matrices are constants. Incorrect initialization may cause large estimation errors or filter divergence. The adaptive extended Kalman filter (AEKF) [9-10] with a noise-adaptive process has therefore produced great progress in SOC estimation. Nevertheless, the performance of the above methods depends highly on the model's accuracy, and thus, the battery parameters must be identified before estimating its state. The existing parameter identification methods mainly contain offline and online parameter identification methods [11]. The former obtains the approximate battery parameters from the voltage information of specified test data combined with circuit analysis. It is difficult to track the operating state of the Li-ion battery over time. Instead, an improved recursive least squares-based algorithm allows for online updating of the model parameters, combined with the estimation algorithm described above, to obtain a more accurate SOC estimation based on ECM.

The capacity determines the amount of energy stored in a lithium-ion battery and is closely related to the battery's SOC. During battery charging, side reactions caused by temperature or aging can deplete the active lithium and cause damage to the electrode material. These factors result in a decrease in capacity. Although these changes are slow, especially after some large changes in SOC [12-13], they still need to be frequently updated in the SOC estimation. Therefore, calculating SOC using only a fixed cell capacitance rating will lead to a small estimation error, which is often overlooked in studies. For example, in [14], even though a fractional-order model for lithium-ion batteries was constructed in SOC estimation that converges to the true value, the variation in capacity was still not considered.

Similarly, capacity/state of health (SOH) estimation methods can be classified into measurement-based, data-based, and model-based methods [15]. Measurement-based methods, such as incremental capacitance analysis (ICA) and differential voltage analysis (DVA) [16], can be used to estimate SOH. Although they can reflect battery aging to obtain an accurate estimate, it is difficult to use them for online estimation of the actual BMS due to equipment and time limitations. Second, data-driven approaches, such as using neural networks to implement estimation and monitoring of battery SOH, rely on a large amount of offline data [17]. Given this, model-based capacity estimation methods have turned out to be an intensely researched topic. Model-based capacity estimation is often performed in conjunction with SOC estimation due to its slow-varying nature [18]. Schwenk et al. [19] used a two-particle filter to estimate SOC and capacity, but crosstalk between the two filters could not be avoided. To address this, some studies have proposed multiple time scales for SOC and capacity [20-21], but superposition interference still exists. In addition, according to the relationship between capacity and SOC, the SOC variation of the preset time interval can be used to calculate the battery capacity [22], but this method is limited by offline detection with unclear interval settings. Zou et al. [23] designed a fourth-order EKF to jointly estimate the SOC and capacity; however, the higher-order filter may lead to a huge computational effort or even instability and does not consider the temperature. In [24], Wang et al. applied AUKF to the third-order classical equations to jointly estimate the capacity and SOC with the help of neural networks to describe the relationship between SOH and battery capacity and temperature, but this classical joint estimation method still suffers from a large computational effort.

To address the above issues, a framework for the joint estimation of capacity and SOC with a low computational cost is presented in this paper. First, this paper uses the VFFRLS algorithm to identify the Thevenin equivalent model parameters, which improves the accuracy of the parameters under complex operating conditions. Subsequently, a simplified model equation with OCV as the observed noise is derived. Combined with this equation, this paper proposes the adaptive extended Kalman filter algorithm with a subregional decay element (ADEKF) to perform the joint estimation of SOC and capacity. Experimental results show that the proposed method achieves a balance between computational complexity and estimation accuracy under uncertainty in the initial SOC value and temperature variation considerations and outperforms the traditional method in terms of overall performance.

2. BATTERY MODEL AND PARAMETER IDENTIFICATION

2.1 Lithium battery model

Currently, the ECM method is widely applied in model-based SOC estimation. It can be classified into several categories, such as the Thevenin model, the Rint model, and the PNGV model [25]. Among them, the Thevenin model can achieve comparable prediction accuracy as the other models but with low model complexity. Thus, it is adopted here to emulate the battery dynamics. As shown in Figure 1, the model contains open-circuit voltage U_{ocv}, an internal ohm resistance R_0, internal polarization resistance R_p and internal polarization resistance C_p.

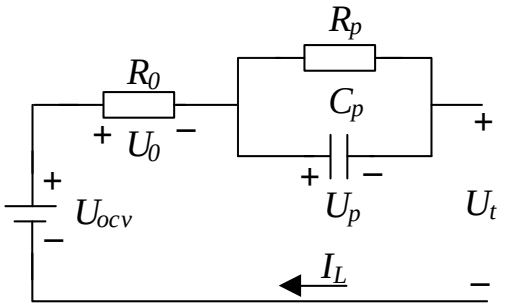

Figure 1. Structure of the Thevenin model

According to Figure 1 and Kirchhoff's theorem, the state-space expression of this model can be obtained as:

$$\begin{cases} \dot{U}_p = -\dfrac{1}{C_p R_p} U_p + \dfrac{1}{C_p} I_L \\ U_t = U_{OCV}(SOC) - U_p - I_L R_o \end{cases} \tag{1}$$

where $U_{ocv}(SOC)$ represents the computed U_{ocv} through the OCV-SOC relationship, U_p denotes the voltage across the polarization resistance, and U_t and I_L are the terminal voltage and the load current, respectively.

The discretized form of this model is derived as follows:

$$\begin{cases} U_{p,k} = U_{p,k-1} \exp\left(-\dfrac{T_s}{C_p R_p}\right) + I_{L,k-1} R_p \left[1 - \exp\left(-\dfrac{T_s}{C_p R_p}\right)\right] \\ U_{t,k} = U_{OCV}\left(SOC_k\right) - U_{p,k} - I_{L,k} R_o \end{cases} \tag{2}$$

In the formula, T_s is the sampling period, and the subscripts k and k-1 indicate the sampling time.

2.2 VFFRLS-based model parameter identification

The forgetting factor with recursive least squares (FFRLS) commonly identifies the model parameters online with real time variation. However, provided that the battery system is working under more sophisticated conditions, it is rarely appropriate to use the constant forgetting factor [26]. Therefore, the VFFRLS algorithm is applied in this paper to improve the performance of online parameter identification, which enables a balance between the parameter convergence speed and tracking error. Above all, we are supposed to conduct some formula transformation.

At sampling time k, the system output is written as:

$$y_k = \phi_k^T \theta_k + \varepsilon \tag{3}$$

where y is the system output and θ, ε and ϕ are the parameter vector, the noise variable, and the information vector, respectively. Based on the research results in [27], we can acquire the relationship between the observed error and the forgetting factor value, which is given as follows:

$$\begin{cases} \lambda(k) = \lambda_{\min} + \left(1 - \lambda_{\min}\right)^{\alpha(k)} \\ \alpha(k) = 2^{\rho e^2(k)} \end{cases} \tag{4}$$

where $e(k)$ is the observation error of the VFFRLS algorithm, λ is the forgetting factor, and λ_{min} is a preset minimum value of the forgetting factor. ρ is a fixed value. Taking 45 ℃ as an example, we set λ_{min} and ρ as 0.74 and 44000, respectively. Combined with the fundamental theory of the least-squares algorithm and after some derivation and transformation, the detailed process of VFFRLS can be summarized as follows:

$$\begin{cases} L_k = P_{k-1}\phi_k \Big/ \left(\lambda + \phi_k^T P_{k-1}\phi_k\right) \\ \hat{\theta}_k = \hat{\theta}_{k-1} + L_k\left(Z_k - \hat{\theta}_{k-1}^T\phi_k\right) \\ P_k = \left(I - L_k\phi_k^T\right)P_{k-1}\Big/\lambda \\ \begin{cases} \lambda(k) = \lambda_{\min} + \left(1 - \lambda_{\min}\right)^{\alpha(k)} \\ \alpha(k) = 2^{\rho e^2(k)} \end{cases} \end{cases} \tag{5}$$

Herein, L is the gain, P denotes the covariance matrix, $\hat{\theta}$ is the estimate of the parameter vector, and I is the identity matrix.

According to Eq. (2), the terminal voltage U_t can be expressed by:

$$U_t(s) = U_{OCV}(s) - I_L(s)\left(\frac{R_p}{1 + C_p R_p s}\right) - I_L(s)R_0 \tag{6}$$

Then, we define E_t as the difference between U_{OCV} and U_t, and the transfer function can be derived by Eq. (6):

$$G_S = \frac{U_t(s) - U_{OCV}(s)}{I_L(s)} = \frac{E_t(s)}{I_L(s)} = -R_0 - \frac{R_p}{1 + C_p R_p s} \tag{7}$$

where s is the transfer function operator. Generally, the bilinear transformation in Eq. (8) is applied to discretize Eq. (7), and Eq. (9) is calculated by:

$$s = \frac{2}{T_s}\frac{1 - z^{-1}}{1 + z^{-1}} \tag{8}$$

$$G\left(z^{-1}\right) = -\frac{\alpha_2 + \alpha_3 z^{-1}}{1 - \alpha_1 z^{-1}} \tag{9}$$

where z means a discretization operator, and the coefficients in the numerator and the denominator are obtained from Eq. (7) and Eq. (9):

$$\begin{cases} \alpha_1 = -\dfrac{1 - 2C_p R_p}{1 + 2C_p R_p} \\ \alpha_2 = -\dfrac{R_0 + R_p + 2C_p R_p R_0}{1 + 2C_p R_p} \\ \alpha_3 = -\dfrac{R_0 + R_p - 2C_p R_p R_0}{1 + 2C_p R_p} \end{cases} \tag{10}$$

Assuming that the variation in OCV at adjacent sampling times can be ignored as a consequence of its slow-varying feature:

$$U_{OCV,k} \approx U_{OCV,k-1} \tag{11}$$

Thus, Eq. (11) can be reformulated as:

$$U_{t,k} = \alpha_1 U_{t,k-1} + (1-\alpha_1) U_{OCV,k} + \alpha_2 I_{L,k} + \alpha_3 I_{L,k-1} \tag{12}$$

Herein, we define the parameter vector $\theta = [\alpha_1 \quad (1-\alpha_1)U_{OCV} \quad \alpha_2 \quad \alpha_3]^T$ and information vector $\phi = [U_{t,k} \quad 1 \quad I_{L,k} \quad I_{L,k-1}]$.

After θ is identified by the VFFRLS, the corresponding model parameters can be immediately acquired from Eq. (13):

$$\begin{cases} R_0 = \dfrac{(1+2\tau)(\alpha_3 - \alpha_2)}{4\tau} \\ R_P = R_0(2\tau - 1) - \alpha_3(1+2\tau) \\ \tau = \dfrac{1+\alpha_1}{2(1-\alpha_1)} \\ U_{OCV} = \dfrac{\alpha_1}{(1-\alpha_1)} \end{cases} \tag{13}$$

In the formula, the model's time constant $\tau = R_P C_P$. As shown in Eq. (13), the OCV can be directly identified if $\alpha_1 \neq 1$, which can easily be derived from Eq. (10).

3. JOINT ONLINE ESTIMATION FOR BATTERY CAPACITY AND SOC

3.1 Joint estimation based on ADEKF

The SOC is generally expressed as the ratio between the residual available capacity and maximum available capacity. Thus, we can obtain the SOC value at time step *k* during the discharging process as follows:

$$SOC_k = SOC_{k-1} - \frac{\eta I_{L,k-1} T_s}{C_{n,k-1}} \tag{14}$$

where η is the coulombic efficiency and $SOC_{k\text{-}1}$ and SOC_k denote the SOC values at time steps *k*-1 and *k*, respectively. $C_{n,k\text{-}1}$ denotes the cell capacity at time step *k*-1 in ampere-seconds.

Capacity is a measurement of the battery SOH, and it is of significance for the SOC to accurately estimate capacity. According to the aforementioned analysis, we propose an innovative low-complexity filter based on the ADEKF considering an assumption of battery characteristics. Primarily, the implementation details of the model equation are described below.

For a nonlinear discrete-time system, the state space model equations can be described as:

State equation:

$$x_k = f(x_{k-1}, u_{k-1}) + w_k \tag{15}$$

Measurement equation:

$$y_k = g(x_k, u_k) + v_k \tag{16}$$

where x_k and y_k represent the state variable and measurement variable at time step *k*, respectively, f is the nonlinear process function, and g is the nonlinear measurement function. u_k is the system input signal, and v_k and w_k are the measurement noise and process noise, respectively. In this paper, since U_{ocv} is not related to U_p, a smaller number of variables can be integrated into the low-order filter. In other words, the state vector is defined as $x = [SOC, Cn]^T$, and we choose $y = U_{ocv}$ in this paper. On this basis, the state equations for the estimation of the capacity and the SOC are given as follows:

$$\begin{cases} C_{n,k} = C_{n,k-1} \\ SOC_k = SOC_{k-1} - \dfrac{\eta I_{k-1} T_s}{C_{n,k-1}} \end{cases} \tag{17}$$

where $C_{n,k}$ denotes the cell capacity at time step k.

Measurement equation:

$$U_{OCV,k} = U_{OCV,k}\left(SOC_k\right) \tag{18}$$

Herein, we regard the OCV identified from VFFRLS as the observation state: $U_{ocv,k}$. $U_{ocv,k}(SOC_k)$ represents the SOC-OCV mapping and is obtained by the standard SOC-OCV test, which will be discussed thoroughly in Section 4.2.

It is worth noting that the OCV curve does not change significantly while the battery capacity decays in an individual cycle. As shown in [28], the change in OCV is only 1.251 mV over 60 discharge cycles for the battery's SOC range of 10% to 80%. Given these characteristics, we can further simplify the Jacobi matrix by decoupling the capacity from U_{ocv} as follows:

$$\frac{\partial U_{ocv,k}\left(SOC_k\right)}{\partial C_{n,k}} = \frac{dU_{ocv,k}\left(SOC_k\right)}{dSOC_k}\frac{dSOC_k}{dC_{n,k}} \approx 0 \tag{19}$$

In practice, the system noise is an uncorrelated nonzero mean Gaussian white series. In this scenario, the AEKF algorithm shows effectiveness and robustness, so it is essential to update it for better joint estimation of capacity and SOC in this paper. The estimation accuracy of the Kalman filter algorithm is determined by two factors: the prediction process and the correction process. The latter is the feedback correction of the observation error by using the mapping of states to observations.

There is a smooth section of the SOC-OCV curve which has such a small gradient that a weak OCV error can cause a large error in SOC. Accordingly, the error feedback needs to be adjusted appropriately when OCV is selected as the measurement noise. Combining the hysteresis of the RLS in the low SOC region [29] and the characteristics of the Kalman filter [30], the subregional decay element is derived for the AEKF in this paper as follows:

$$\beta = \begin{cases} 10^{-3} & if \quad t \geq T_{soc=0.2} \parallel \Delta U_{ocv} \geq e_{\min} \\ 1 & else \end{cases} \tag{20}$$

$$H_k = \frac{1}{M}\sum_{i=k-M+1}^{k} e_i e_i^T \tag{21}$$

Here, T_{soc} is the moment when SOC equals 20%, and β and e_{min} are the subregional decay element and the minimum error based on a priori estimation, respectively. The ΔU_{ocv} refers to the error between the true value and the measured value. That is, the transfer parameters should be reduced to the β multiples of the original in the low SOC region, and the moments of large OCV should be reduced accordingly in the high SOC region.

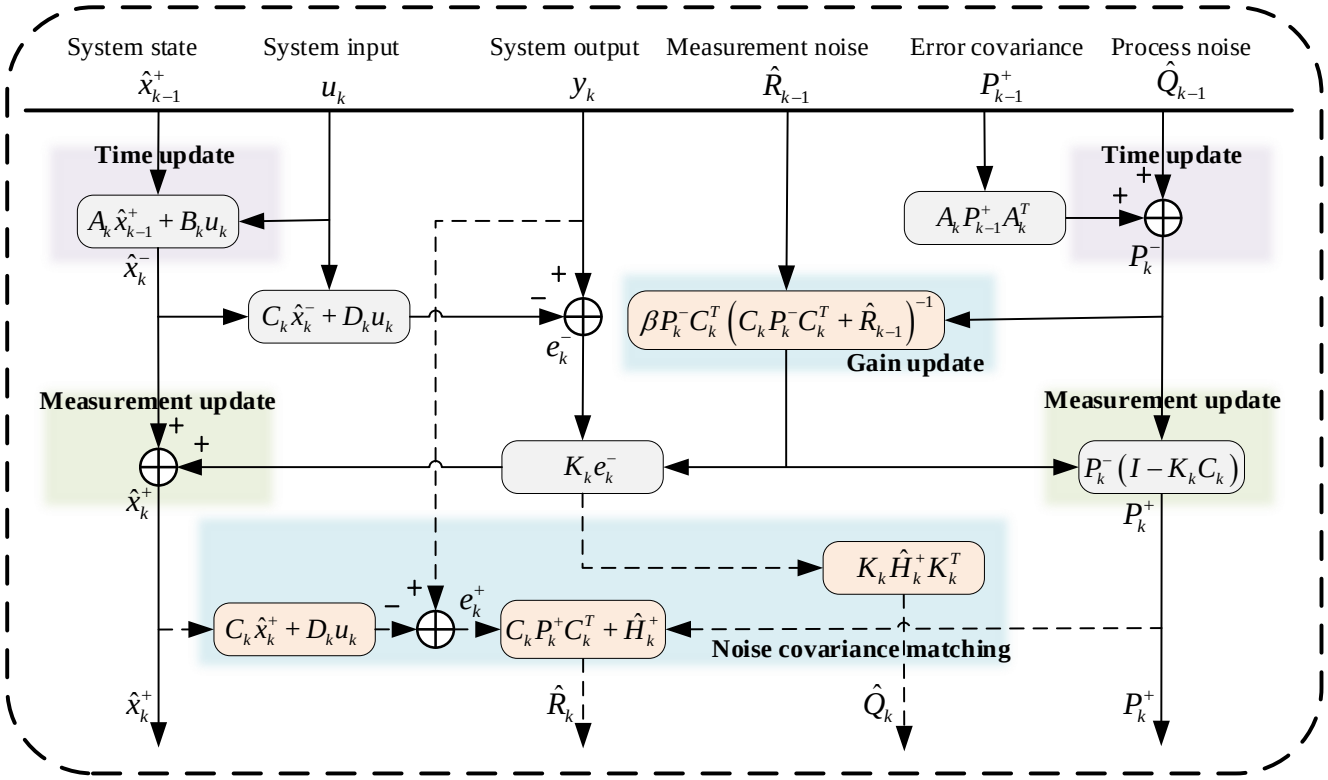

Figure 2. The detailed flowchart for the ADEKF Algorithm.

The detailed flowchart of the ADEKF algorithm is shown in Figure 2. The symbol "^" indicates the estimated value. B and D in Figure 2 are the Jacobi matrices involved in Eq. (2). The superscripts "+" and "–" denote the a priori predicted and the a posteriori updated values, respectively.

The solid line indicates the process of the traditional Kalman filter. Meanwhile, the dashed line denotes the dynamic update of the noise covariance. The conventional AEKF algorithm enables adaptive matching of the system process and measurement noise covariances. Based on updating the noise covariance through the moving average window, the process measurement covariance is calculated using the new interest matrix e_k with the corresponding $\widehat{H}_k^-$, as shown in Eq. (22). To ensure the positivity of the matrix, the measurement noise covariance subsequently applies the residual error to calculate the corresponding variance $\widehat{H}_k^+$. Of note, when the low SOC range and other range-new interest matrices are larger than the set value, this paper adds a decay factor for the gain update region. This not only allows the optimal value of the algorithm to better track the SOC-OCV mapping but also enhances the robustness of the new low-order filter.

3.2 The joint-estimation process

Figure 3 shows a supplementary framework for the joint estimation method. First, the battery model parameters, including U_{OCV}, are identified online by VFFRLS. Next, the identified OCV is passed to the ADEKF in real time to measure the variables.

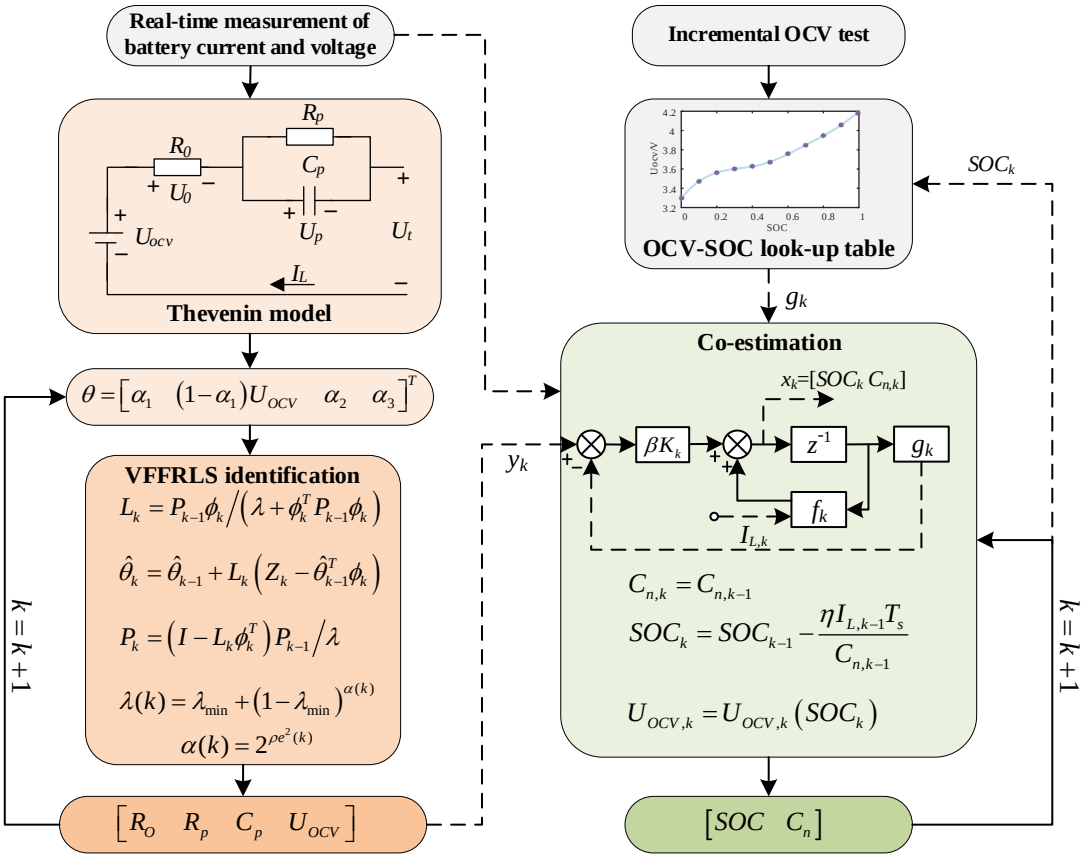

Figure 3. The detailed flowchart for the SOC and capacity estimation.

The proposed algorithm integrates only the capacity and SOC in the state vector. Through the SOC-OCV relationship, the estimated SOC involving the capacity value at the previous moment is used to obtain the OCV estimate value. Error correction between the OCV estimate and reference value are combined with β-gain for state correction. Moreover, the decoupling of capacity from U_{OCV} in the proposed algorithm further reduces the computational burden with destabilization.

Theoretically, the proposed method reduces the computational complexity, and it is more significant for encountering higher-order RC models or considerable aging cycles. The precision and robustness of the proposed method can be verified exactly by the dataset in the following section. In addition, its performance will be confirmed compared to the classical third-order estimator.

Furthermore, the performance of the algorithms proposed in this work is also verified by comparison with that obtained for current mainstream algorithms, such as the Multi-timescale EKF, the AVMT EKF, the Hybrid model, the Triple PI model and the Dual-AEKF algorithms which is the most common classical method. The models and claims of the above joint estimation algorithms are described briefly as below. The Multi-timescale EKF algorithm utilizes alternating SOC and capacity estimation at different time scales of the EKF. To address the problem of different variation characteristics of battery SOC and capacity, the AVMT EKF algorithm proposes a new adaptive variable multi-timescale framework. Although this approach can reduce the effect of current drift, using recursive total least squares (RTLS) for capacity estimation still leads to large error. The Hybrid model uses the estimated

SOC interval accumulation to calculate the capacity, after which the estimated capacity is provided to the next SOC estimation with the capacity update. Obviously, the moment selection and length of the interval have an impact on the accuracy of the algorithm. The Triple PI model uses three observers for the joint estimation of capacity, SOC and resistance. Similar to the higher-order EKF, this model is also less resistant to disturbances in the initial iterations. The last method is the Dual-AEKF algorithm, where the capacity is estimated using the first AEKF, and it is transferred to the second AEKF to complete the SOC estimation. And This model still cannot avoid the interference of data transmission from two filters.

4. EXPERIMENTAL RESULTS AND ANALYSIS

To effectively validate the model parameter identification method and the novel second-order filtering algorithm proposed in this paper, this section employs an INR 18650-20R lithium-ion battery. Its main parameters are displayed in Table 1. The experimental data are obtained from the open cell dataset of the Center for Advanced Life Cycle Engineering at the University of Maryland.

Table 1. The specifications of the tested lithium-ion battery

Characteristics	value	Characteristics	value
Nominal capacity/Ah	2	Lower cutoff voltage/V	2.5
Nominal voltage/V	0.32	Weight/g	45
Upper cutoff voltage/V	4.2	Temperature range/℃	-20~60

In this paper, the incremental OCV test is selected to track the SOC-OCV mapping. Meanwhile, the nonlinearity of this relationship is highlighted by the fitting tool in MATLAB. The root mean squared error (RMSE) is used to evaluate the fitting accuracy, as shown in Eq. (22).

$$RMSE = \sqrt{\frac{\sum_{i=1}^{n}(w_i - \hat{w}_i)^2}{n}} \tag{22}$$

Herein, w_i and $\hat{w}_i$ denote the predicted and reference values, respectively. n represents the number of data points. For instance, the OCV-SOC relationship was fitted using polynomial functions of different orders for data at 25 ℃, whose RMSE is shown in Figure 4.

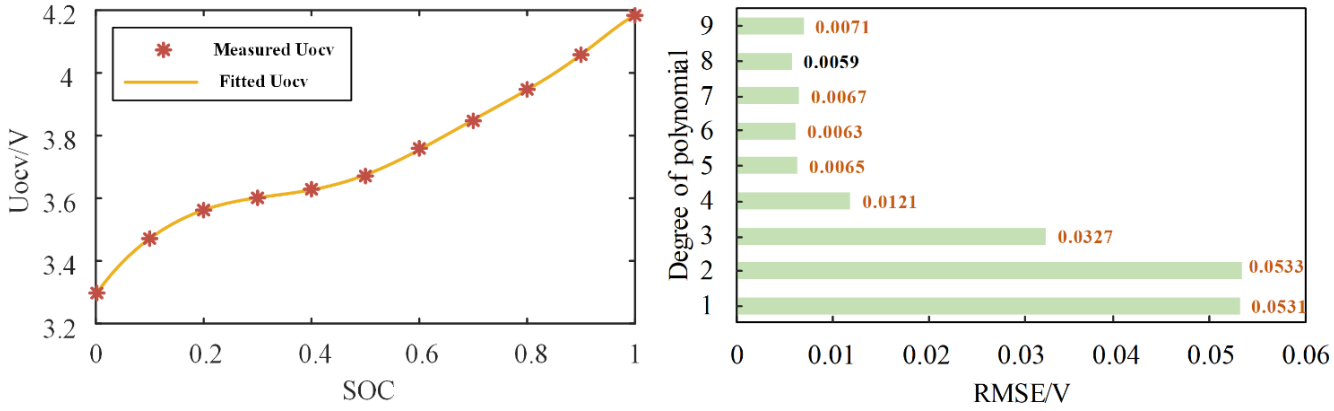

Figure 4. The open circuit voltage fitting curve and RMSE of different order functions.

Finally, we determined the eighth-order fitted curve with a minimum RMSE of 0.0059 V to describe the relationship between OCV and SOC. The fitted OCV-SOC curve is shown in Figure 4, and then the function g(x) mentioned in subsection 3.2 can be determined, whose corresponding function is presented as:

$$g(x) = k_8x^8 + k_7x^7 + k_6x^6 + k_5x^5 + k_4x^4 + k_3x^3 + k_2x^2 + k_1x + k_0 \qquad (23)$$

where x is SOC and g is the function between U_{ocv} and SOC. The optimal coefficients of the above function with respect to other temperatures are also listed in Table 2.

Table 2. The optimal coefficients of the SOC-OCV function at various temperatures

Temperature/℃	k_0	k_1	k_2	k_3	k_4	k_5	k_6	k_7	k_8
0	-46.46	142	-138.9	18.98	46.4	-25.23	3.303	0.622	3.456
25	-175.5	689.9	-1097	906.1	-422.5	118.2	-22.22	3.416	3.264
45	-225.4	899.4	-1456	1230	-584.6	161.8	-27.58	3.558	3.277

FUDS is a typical dynamic transient driving cycle which is more complex than DST. The data are extracted from FUDS with respect to SOC's 10% to 80% range, which is the classic operating state of the battery. Hence, the FUDS contains 8-10 cycles at various temperatures, such as 0 ℃, 25 ℃ and 45 ℃, and their current and voltage profiles are shown in Figure 5.

At essentially the same current excitation, the discharge time of the voltage at 45 °C is longest, while the discharge time of the corresponding voltage at 0 °C is the shortest. This indicates that when the ambient temperature is lower, the chemical reaction rate and activity of the battery are lower, resulting in insufficient battery discharge. Notably, when the temperature changes, the available capacity of the battery also changes, which should be considered in the SOC estimation.

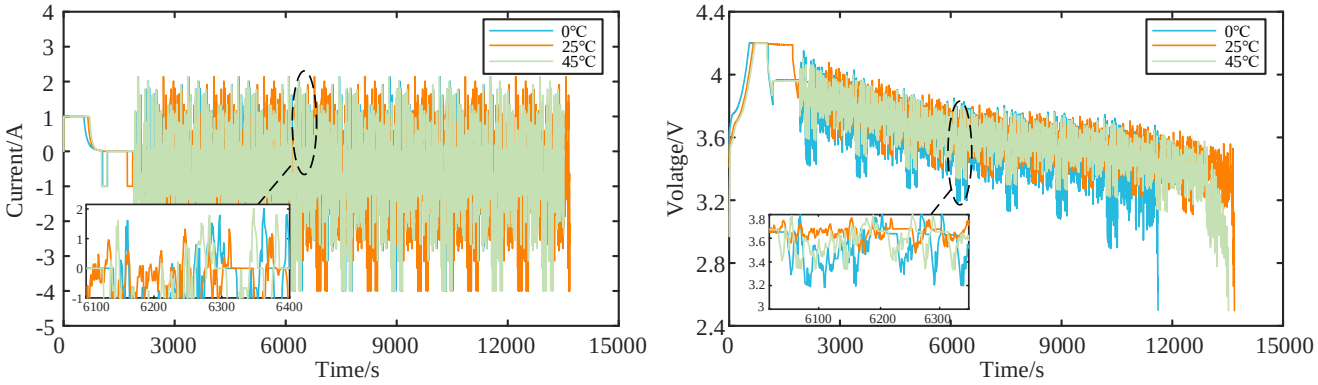

Figure 5. Current and voltage profile of the FUDS test at various temperatures.

4.1 Modeling and parameter identification

According to the above parameter identification method, the Thevenin's model parameters can be obtained under the FUDS operating conditions at 25 °C, as shown in Figure 6. It can be seen that R_0 changes little and tends to increase with the use of the battery, while R_p and C_p tend to decrease. This also indicates that RLS does not describe the battery polarization in the low SOC region.

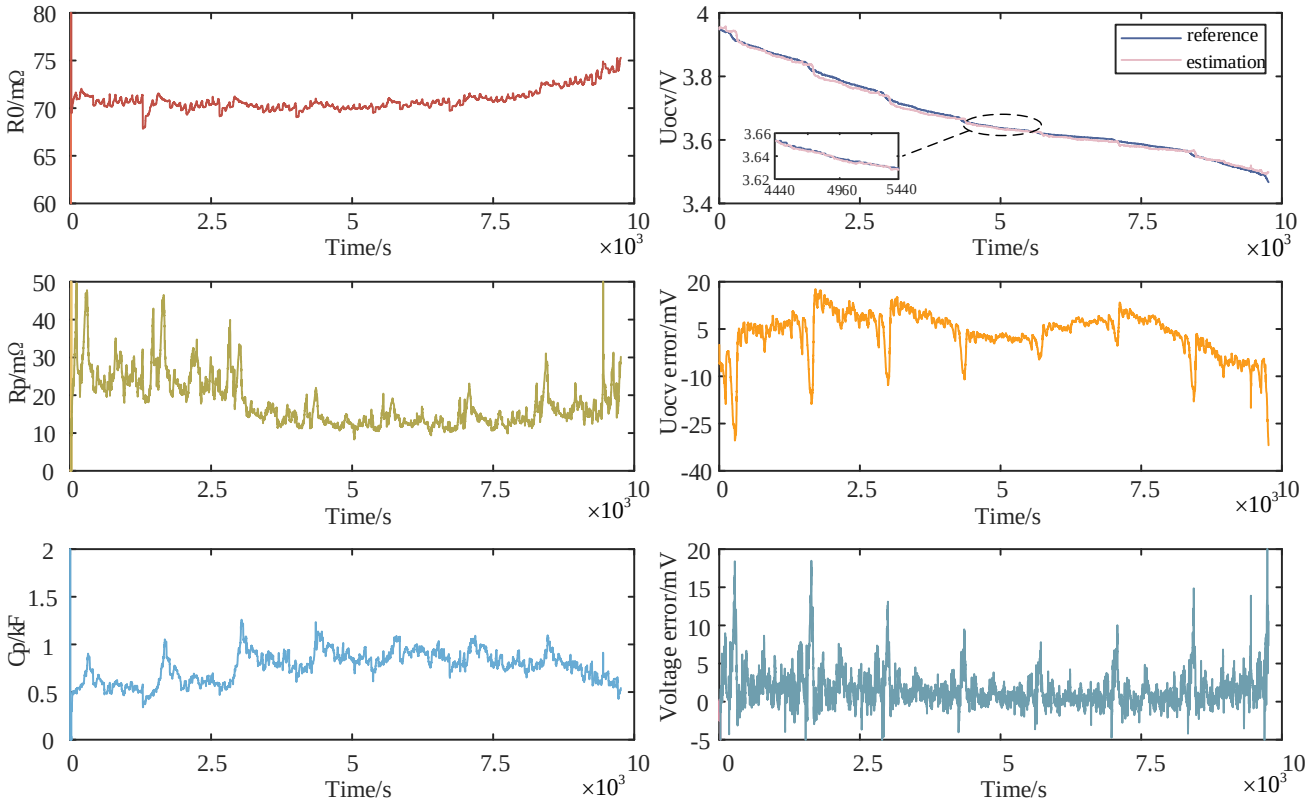

Figure 6. Parameter identification results at 25℃ based on VFFRLS.

The model parameters are time-varying due to changes in electrolyte ionic conductivity and the concentration of lithium ions if the battery discharges. This confirms the need for online parameter identification. Furthermore, the reference OCV is calculated by the estimated SOC combined with the SOC-OCV relationship. The results of the comparison between the considered measured OCV and the reference OCV are displayed in Figure 6. It is clear that the error between them can be limited to the range of -20 mV to 30 mV. Therefore, the identified OCV has the potential to be treated as a measurement variable for the filter.

Finally, as shown in Figure 6, the error bands between the measured and predicted voltages are mostly in the range of -5 mV to 10 mV. This means that the developed cell model is able to track the dynamic characteristics of the cell very well. This has also been verified for FUDS operating conditions at other temperatures.

4.2 Precision of the joint estimation

In this paper, the convergence time and the estimation error after convergence are used as performance measures to quantitatively evaluate both algorithms. The convergence time is defined as the time when the estimated SOC/capacity starts to stabilize within a 5%/10% error range. Thus, based on the previous information about FUDS at 25 ° C, this section implements the joint estimation of SOC and capacity when SOC is initially uncertain. The reference SOC is obtained by the coulomb counting method, and the initial SOC value is set to 80%. Figure 7 depicts the joint estimation results and convergence trends for SOC and capacity using two initial SOC values (preset to 70% and 60%). Meanwhile, to verify the accuracy and robustness of the method proposed in this work, the RMSE and the mean absolute error (MAE) are applied to evaluate the SOC and capacity indicators of the proposed method performance. These indicators are defined as follows:

$$MAE = \frac{1}{n}\sum_{i=1}^{n}\left|w_i - \hat{w}_i\right| \tag{24}$$

$$C_{RE} = \frac{\left|C_{est} - C_{ref}\right|}{C_{ref}} \times 100\% \tag{25}$$

where $w_i$represents the actual value and $\hat{w}_i$ represents the predicted value. C_{RE} refers to the relative error of battery capacity. Meanwhile, C_{est} and C_{ref} denote the estimated value and the reference value of the capacity, respectively.

It can be concluded from the enlarged local plot of the SOC estimate that the estimated SOC converges to the reference value in 25 s even though the initial SOC value is imprecise. Furthermore, the error range between the reference SOC and the estimated SOC is roughly controlled to ±1.5%. This paper uses Eq. (25) as the basis for capacity evaluation, the initial value is set to the rated capacity, and the proposed algorithm can converge to the actual reference capacity of 1.95 Ah in 3600 s.

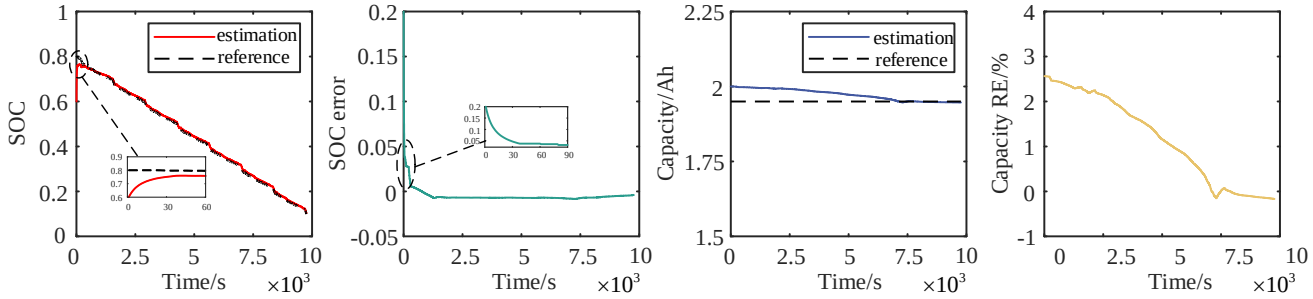

(a) the joint estimation results for SOC and Capacity with initial SOC as 0.6

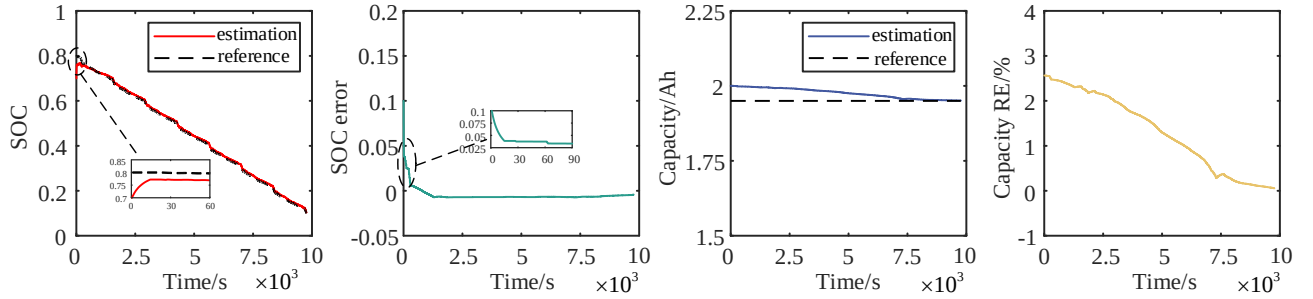

(b) the joint estimation results for SOC and Capacity with initial SOC as 0.7

Figure 7. SOC estimation results and errors with incorrect initial SOC values

The adjusted available capacity is used for the next step of updating the SOC status. As a result, the MAE and RMSE of the SOC estimate do not exceed 1%, while the MAE is controlled to 1.5%, as shown in Table 3. Overall, the algorithm exhibits good convergence and robustness under incorrect initial SOC values.

Table 3. SOC estimation without correct initial SOC values

Initial parameter values		SOC estimation results		
Available Capacity/A • s	SOC_0/%	Convergence time/s	MAE/%	RMSE/%
7200	60	35	0.72	0.96
7200	70	11	0.69	0.80

4.3 Robustness against various temperature effects

To verify the effect of ambient temperature on this algorithm, this paper compares and analyzes the estimation results of the proposed algorithm at room temperature and in high- and low-temperature cases, as shown in Figure 8. At high temperature, the activity of lithium ions inside the battery is increased, so the capacity convergence state at 45℃ is better than that at 25℃. However, since the initial capacity at room temperature is defined as the rated capacity, which deviates from the actual initial capacity of the battery, there is a small fluctuation, but it still eventually converges to the reference value. At 45 °C, the use of a random initial capacity also does not affect the ADEKF algorithm convergence to

the actual capacity value. This shows that the proposed algorithm can achieve good estimation accuracy even when the initial capacity is unknown.

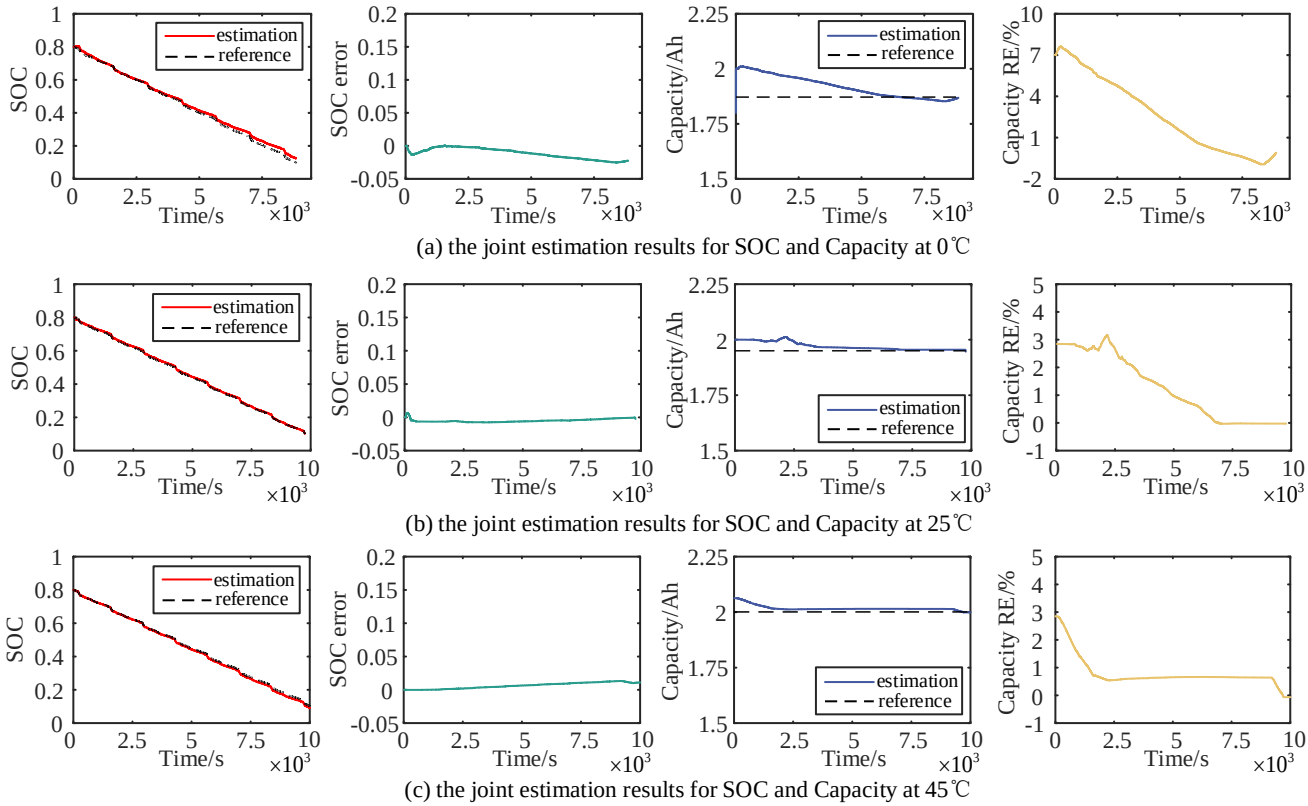

Figure 8. The joint estimation results and errors at various operating temperatures.

As shown in Table 4, the proposed joint estimation method can better combat temperature fluctuations and limit the estimation error bands of SOC and capacity to 1% and 3%, respectively. In addition, even though the Thevenin model does not respond well to the low-temperature battery polarization characteristics, the ADEKF algorithm can still achieve good estimation results, with the SOC is within 2%. This also shows that adding a decay factor in the Kalman gain update process in combination with the RLS features improves the results.

Table 4. Calculation results of the SOC estimation against operating temperature variation.

Temperature/℃	Initial parameter values		SOC estimation results	
	Available Capacity/A • s	SOC_0/%	MAE/%	RMSE/%
0	7200	80	1.26	1.55
25	7200	80	0.53	0.56
45	7380	80	0.63	0.78

4.4 Superiority of the joint estimation algorithm

To further verify the superiority of the proposed method, the algorithm is compared from two perspectives: firstly, the suitability of the ADEKF to the reduced-order equation of state, secondly, the proposed overall framework is realized for comparison with the traditional method.

In this section, the superiority of the proposed method is regarded as 'L-ADEKF', and the simplified low-order equation of state combined with AEKF is named 'L-AEKF'. The traditional high-order filter based on AEKF is regarded as 'H-AEKF', which also represents the traditional method. The three algorithms are compared using the FUDS data at 25 °C and with the initial SOC randomly set to 0.72 and the initial capacity set to 2 Ah.

The estimated results of SOC are shown in Figure 9. Obviously, both the proposed method and L-AEKF converge to the reference SOC within 60 s, while the H-AEKF performance is relatively weak with the initial SOC error. Meanwhile, the L-ADEKF obtains a suitable Kalman gain in the estimation process due to the addition of the attenuation factor, which minimizes the MAE and RMSE of the SOC of this algorithm. To analyze the causes of this phenomenon in SOC estimation, the capacity estimation results of these three methods need to be compared. Intuitively, the capacity error curve of L-AEKF is much more drastic, and it is difficult to determine the convergence time. This demonstrates that the AEKF algorithm does not match well with the proposed simplified state equation due to the shortage of RLS. However, it converges gradually to the true value even over a long time of 8000 s. In contrast, L-ADEKF shows a more stable convergence ability, keeping the relative error within 2.5%. In addition, the traditional algorithm named H-AEKF shows general estimation results due to the instability of the higher-order EKF itself.

To further evaluate the estimation results, it can be seen from Table 5 that the MAE and RMSE of the proposed algorithm in SOC estimation are below 0.8% and 2.2%, which are approximately 1.5% and 1.3% lower than those of the traditional algorithm, respectively. Meanwhile, the convergence time is reduced by 33%.In terms of capacity estimation, the MAE and RMSE of the proposed algorithm are controlled within 2.2%, which is approximately 1.6% less than that of the traditional algorithm.

Table 5. Performance comparison of the proposed and traditional methods with an unknown initial state

	SOC estimation		Capacity estimation	
	L- ADEKF	H-AEKF	L- ADEKF	H-AEKF
MAE/%	0.59	2.16	1.72	3.29
RMSE/%	0.76	2.55	2.11	3.82
Convergence time/s	51	156	4000	6800
CPU time/μs	97	143	——	——

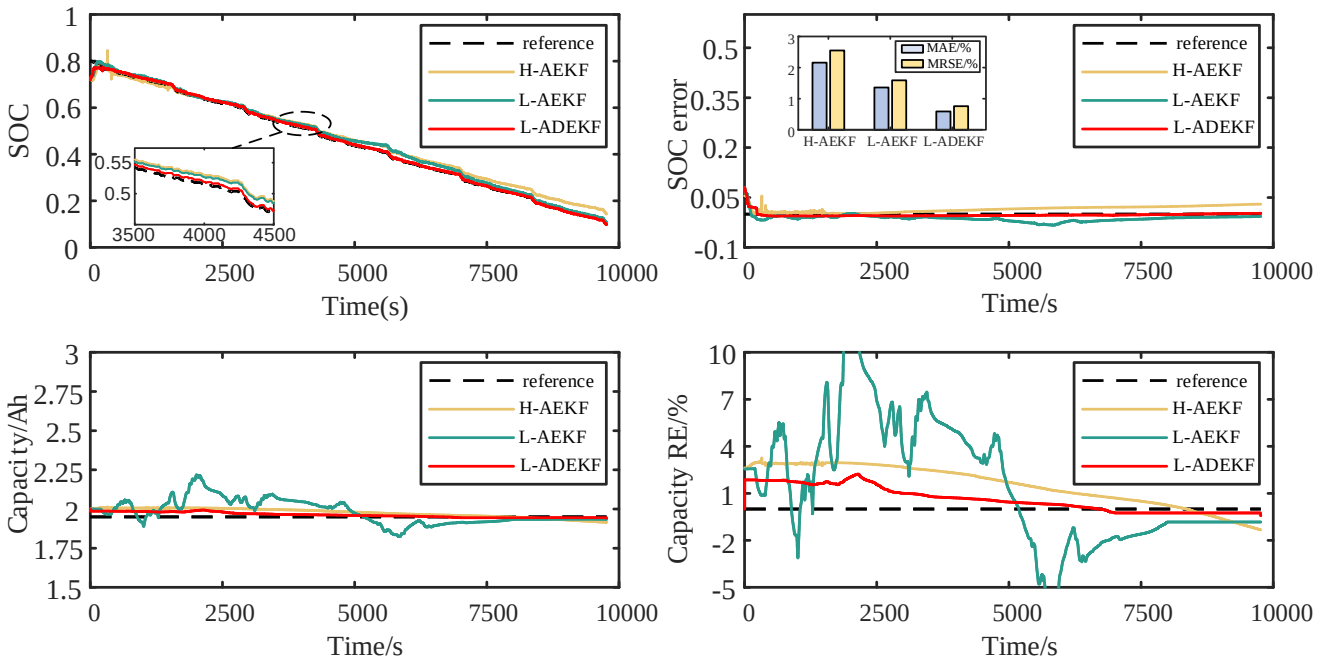

Figure 9. SOC and capacity estimation results and errors of the three methods

4.5. Model Comparative Analysis

To verify the performance of the proposed algorithm, we compare it with the some mainstream joint-estimation algorithm mentioned in Subsection 3. The comparison results are presented in Table 6. It is worth noting that we use the 25 ℃ data from the reference literature for the comparison. None indicates that the reference result is not given in this literature. We can observe that the MAE of the SOC estimation is the lowest for the algorithm proposed in this paper. On the contrary, the estimation result of the Multi-timescale EKF is the worst, which has an RMSE of SOC and capacity greater than 3%. Based on the first model, the AVMT EKF algorithm proposes a new adaptive variable multi-timescale framework. Thus, its convergence time is reduced by 40% than the Multi-timescale EKF model. The Dual-AEKF method has a 1.7% improvement in SOC accuracy over the former approximately. However, the capacity convergence time of this method is as much as 8000 s due to the cross-talk effect of the double EKF, and the algorithm fluctuates in the late stage of the estimation. The Hybrid model can obtain the capacity based on the OCV with accumulated charge, so although the fastest capacity convergence speed is achieved, the uncertainty of the interval time leads to a reduction in the SOC estimation accuracy and algorithm flexibility. The Triple PI model achieves better accuracy for the joint estimation of battery SOC, capacity and resistance based on a ternary proportional integral observer. But its structure is too complex for practical application.

In summary, compared with the above algorithms, the algorithm proposed in this paper shows better performance in terms of accuracy and convergence speed and achieves simple and stable capacity and SOC joint-estimation, which is important for engineering applications.

Table 6. Error analysis for the proposed model compared to that for other joint estimation models

Joint-estimation Model	SOC estimation		Capacity estimation	
	MAE/%	RMSE/%	RMSE/%	Convergence time/s
Multi-timescale EKF[31]	None	3.01	4.20	12000
AVMT EKF[32]	3.15	None	3.99	7200
Hybrid model[33]	0.96	1.25	2.11	3400
Triple PI model [34]	0.81	0.95	1.67	None
Dual-AEKF[35]	0.78	0.91	1.65	8700
ADEKF[this work]	0.54	0.56	1.62	4000

5. CONCLUSION

To reduce the computational complexity and improve the accuracy of online joint battery estimation, a simplified integrated filter based on the ADEKF algorithm for online joint estimation of SOC and capacity is proposed in this paper, which considers multitemperature conditions and different initial values of batteries. The proposed joint estimation method is validated under FUDS conditions. The main contributions are as follows:

(1) The simplified reduced-order equation of state for the battery is derived to reduce the computational complexity of the model-based SOC estimation according to the battery characteristics.

(2) The gain mismatch problem in the online capacity estimation process of the proposed state equation is solved. The AEKF is improved by a subregional decay element factor. The initial capacity tolerance of online estimation of SOC for Li-ion batteries is improved, which makes the Li-ion battery more adaptable to the actual working conditions with variable temperature.

(3) By comparing the MAE and RMSE of SOC and the capacity of other joint estimation methods in cases of random initial values, the method proposed in this work has the fastest convergence speed and the smallest estimation accuracy, which confirms the effectiveness of the joint estimation method. Moreover, it is seen that the proposed method has improved computational quantity and accuracy. In future work, we will explore the sensitivity analysis of additional factors on the battery state and focus on finding advanced intelligent algorithms.

CONFLICTS OF INTEREST

The authors declare that there is no potential conflict of interest involved in this writing process.

ACKNOWLEDGMENTS

Project Supported by National Natural Science Foundation of China 52177184

References

1. A. S. Mogodal, and K. M. Zohdy, *Int J Electrochem Sci.*, 15 (2020) 1128.
2. R. Xiong, Y. Pan, W. Shen, H. Li, and F. Sun, *Renewable and Sustainable Energy Reviews* , 131(2020) 110048.
3. P. Shen, M. G. Ouyang, L. G. Lu, J. Q. Li,snd X. N. Feng, *IEEE Trans. Veh. Technol*, 67 (2017)

92.
4. R. Xiong, J. P. Tian, W. X. Shen, and F. C. Sun. *IEEE Trans. Veh. Technol*, 68 (2019) 4130.
5. J. F. Yang, W. X. Huang, B. Xia, C. Mi, *Applied Energy*, 237 (2019) 682.
6. X Li, Z Wang,L Zhang, *Energy*, 174 (2019), 33.
7. M. Kwak, B. Lkhagvasuren, H. S. Jin. and G. Seo. *Int J Electrochem Sci.*, 17 (2022) 2.
8. C. Jiang, S. L. Wang, B. Wu, C. Fernandez, X. Xiong, and J. Coffin-Ken, *Energy*, 219 (2021) 231.
9. X. L. Dong, C. P. Zhang, J. C. Jiang, *Energy Procedia*, 152 (2018) 520.
10. Y. F. Guo, Z. S. Zhao, L. M. Huang, *Energy Procedia*, 105 (2017) 4146.
11. R. Xiong, L. Li, Q. Yu, Q. Jin, and R. Yang.. *J. Clean. Prod.*, 249 (2020) 119380.
12. X. Li, Z. Wang, J. Yan, *J. Power Sources*, 421 (2019) 56.
13. X. Li, Z. Wang, L. Zhang, C. Zou, D.D. Dorrell, *J. Power Sources*, 410 (2019) 106.
14. R. Xiao, J. Shen, X. Li, W. Yan, E. Pan, and Z. Chen. *Energies*, 9 (2016) 184.
15. H. H. Pan. Z. Q. Lü, H. M. Wang, H. Y. Wei, L. Chen, *Energy*, 160(2018) 466.
16. J. Tian, R. Xiong, Q. Yu, *IEEE Trans. Ind. Electron.*, 66 (2018) 1576.
17. X. Y. Li, Z. P. Wang, and L. Zhang, *Energy*, 174 (2019) 33.
18. L. Y. Ling, Y. Wei, *IEEE ACCESS*, 9 (2021) 47588.
19. S. Schwunk, N. Armbruster, S. Straub, et al., *J. Power Sources*, 239 (2013) 705.
20. P. Shrivastava, T. K. Soon, M. Y. I. Bin Idris, S. Mekhilef, and S.B.R.S. Adnan, *Int. J. Energy Res.*, 46 (2022) 10704.
21. C. Chen, R. Xiong, W. Shen, *IEEE Trans. Power Electron.*, 33 (2018) 332.
22. S. Li, `K. Li, E. Xiao, and C. K. Wong, *IEEE Trans. Ind. Electron.*, 67 (2020) 8484.
23. Y. Zou, X. S. Hu, H. M. Ma, and S. E. Li, *J. Power Sources*, 273 (2015) 793.
24. C. Y. Wang, N. X. Cui, Z. R. Cui, H, T, Yuan, and C. H. Zhang, *J Energy Storage*, 53 (2022) 105.
25. X. Lai, W. K. Gao, Y. J. Zheng, M. G. Ouyang, J. Q. Li, X. B. Han, and L. Zhou, *Electrochim. Acta*, 295 (2019) 1057.
26. L. Lu, H. Zhao,and B. Chen, *IEEE Trans. Circuits Syst. II Express Briefs*, 63 (2016) 588.
27. Z. Lao, B. Xia, W. Wang, W. Sun, Y. Lai, and M. Wang, *Energie*s,11 (2018) 1358.
28. Y. J. Zheng, Y. F. Cui, X. B. Han, H. F. Dai, and M. G. Ouyang, *J Energy Storage*, 44 (2021) 10348.
29. Z. B. Wei, C. F. Zou, F. Leng, B. H. Soong, K. J. Tseng, *IEEE Trans. Ind. Electron*, 65 (2018) 1336.
30. L. M. Wang, D. Lu, Q. Liu, L. Liu, and X. L. Zhao, *Electrochim. Acta*, 296 (2019) 1009.
31. C. Hu, B. D. Youn, and J. Chung, *Appl.Energy*, 92 (2012)694.
32. B. Jiang, H. F. Dai,X. Z. Wei, and T. J. Xu, *Appl.Energy*, 253 (2019) 11369.
33. X. L. Yang, Y. J. Chen, B. Li, and D. Luo, *Energy*, 191 (2020) 116509.
34. L. F. Zheng, L. Zhang, J. G. Zhu, G. X. Wang, and J. C. Jiang, *Appl.Energy*, 180 (2016) 424.
35. R. X. Xiao, Y. W. Hu, and X. G. Jia, *Energy*, 243 (2021) 123072.